

Hari Vasudevan

Department of Mechanical Engineering and
Materials Science,
Yale University,
New Haven, CT 06511
e-mail: hari.vasudevan@yale.edu

Aaron M. Dollar

Assistant Professor
Department of Mechanical Engineering and
Materials Science,
Yale University,
New Haven, CT 06511
e-mail: aaron.dollar@yale.edu

John B. Morrell

Assistant Professor
Department of Mechanical Engineering and
Materials Science,
Yale University,
New Haven, CT 06511
e-mail: john.morrell@alum.mit.edu

Design for Control of Wheeled Inverted Pendulum Platforms

In this paper, we study five aspects of design for wheeled inverted pendulum (WIP) platforms with the aim of understanding the effect of design choices on the balancing performance. First, we demonstrate analytically and experimentally the effect of soft visco-elastic tires on a WIP showing that the use of soft tires enhances balancing performance. Next, we study the effect of pitch rate and wheel velocity filters on WIP performance and make suggestions for design of filters. We then describe a self-tuning limit cycle compensation algorithm and experimentally verify its operation. Subsequently, we present an analytical simulation to study the effects of torque and velocity control of WIP motors and describe the tradeoffs between the control methodologies in various application scenarios. Finally, to understand if motor gearing can be an efficient alternative to bigger and more expensive direct drive motors, we analyze the effect of motor gearing on WIP dynamics. Our aim is to describe electromechanical design tradeoffs appropriately, so a WIP can be designed and constructed with minimal iterative experimentation.
[DOI: 10.1115/1.4029401]

1 Introduction

The inverted pendulum has widely established itself in technical literature as a platform for demonstration of control theory and practice. A relatively recent offshoot of the classical inverted pendulum is the WIP, popularized in contemporary culture by the Segway Personal Transporter [1,2]. There have been other WIPs of varying architectures that have been successfully designed and constructed. Perhaps the first implementation of a WIP is described by Nakajima et al. [3] and Ha and Yuta [4]. Another WIP was described by Grasser et al. [5] and there are numerous other examples and variants [6,7] of WIPs used as teaching and research platforms. The Ballbot [8–10] perhaps deserves a special mention as an omni-directional WIP that balances on a sphere.

The performance of a WIP is greatly affected by its electromechanical design and construction. Yet, models for WIPs do not account for the full complexity of the construction of the platform. Most models use four states, the minimum necessary to describe WIP dynamics with a linear model. As a result, feedback gains computed via linear quadratic regulator (LQR), pole placement, or other techniques do not result in desired performance. For example, Lauwers et al. [8] derive stable LQR feedback gains for the Ballbot; however, they report having to manually adjust one of the gain terms to be able to balance successfully without limit cycling. Grasser et al. [5] derive their gains using pole placement and use experimental data to justify their selection of poles; however, the authors also describe the presence of backlash chattering on higher gains. Akesson et al. [7] describe the addition of a hysteresis based friction compensation term to the standard full state feedback controller to avoid limit cycling. In a series of papers [11–14] dealing with parametric and frictional nonlinearities in WIPs, authors Li, Yang, and Zhang describe a set of adaptive control techniques in conjunction with learning systems such as neural networks and support vector machine to design stable bounded controllers.

In this paper, we address the question of WIP design. Specifically, we model five design choices that influence WIP performance:

- (1) effect of tire visco-elasticity on balancing behavior
- (2) effect of velocity filters
- (3) limit cycle compensation for WIPs
- (4) effect of voltage versus current control for DC motors in WIPs
- (5) effect of motor gearing

In particular, we study how the above design choices affect performance of WIPs. We do not intend to derive complete mathematical models/proofs of the above aspects of design, rather we study design tradeoffs that affect performance. Our goal is to provide insight that enables the WIP designer to develop a machine best suited to his or her application. A block diagram of the architecture of a typical WIP is shown in Fig. 1, highlighting thematically the design choices under investigation in this paper.

We organize this paper as follows: first, we describe our experimental platform and its architecture. We then describe the analytical and experimental methodology we use to make comparisons. Following this, we study the effects of each of the WIP design aspects listed above. We then proceed to discuss the implications of our results on the design of WIPs and finally we conclude by discussing possible avenues of future investigation.

2 Experimental Platform

Our balancing machine “Charlie” is shown in Fig. 2(a). Charlie is a “cluster wheel” balancing machine with three wheels on each

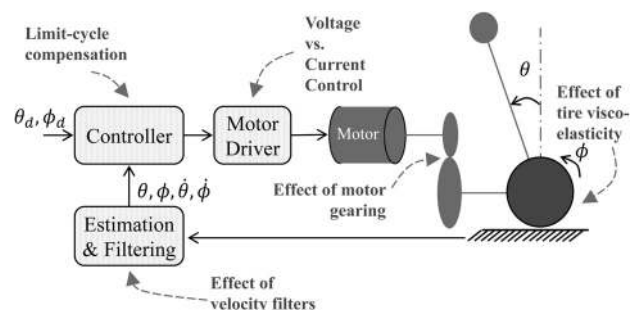


Fig. 1 Block diagram of system architecture with aspects of WIP design addressed in this paper highlighted with arrows

Contributed by the Mechanisms and Robotics Committee of ASME for publication in the JOURNAL OF MECHANISMS AND ROBOTICS. Manuscript received August 15, 2013; final manuscript received November 24, 2014; published online March 11, 2015. Assoc. Editor: Xianmin Zhang.

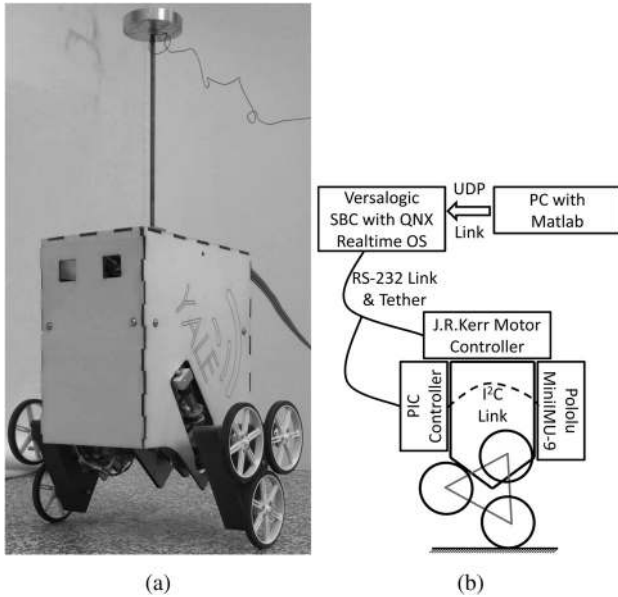


Fig. 2 (a) Charlie—balancing and (b) system architecture

side of the vehicle arranged in a triangular cluster. This is so designed to allow the robot to balance on two wheels and also rest statically stable on four wheels. While Charlie can transition between two and four wheel modes, we solely describe the two wheel balancing behavior in this paper.

Mechanical movement of wheels is controlled using pulse-width modulated (PWM) voltages. The drive system consists of a series of gear heads and timing belts attached to the motors and wheels. The drive system is geared and nonbackdrivable. Note that while we can independently control wheels on either side of the robot, for the purposes of this paper, we link them mechanically with a common drive axle to avoid out-of-plane motions and to examine dynamics of interest.

The robot is controlled via a tether which is suspended from the ceiling to minimize disturbance forces. All motor control and sensor data is sent over two RS-232 links. One link interfaces with a peripheral interface controller microcontroller which transmits inertial measurement unit data to the control personal computer (PC), the other link is connected to the motor controllers. The motors are driven via motor control modules (PIC-Servo SC, Jefferey Kerr, Berkeley, CA) on board the robot and batteries are also carried on board. A PC issues supervisory commands over a user datagram protocol link to the Control PC, this link is used for high level commands such as commanding cluster angle changes and for logging data from the robot. A schematic representation of the system architecture is described in Fig. 2(b).

3 Comparison Methodology

In making performance comparisons for a WIP, we first identify a performance metric. The closed loop performance of a WIP, such as rise time, overshoot, etc., is determined by the location of the closed loop poles. To compare analytically the performance of a WIP over variations in tire damping, gearing ratio, and motor control schemes, we compute closed loop gains required to maintain fixed pole locations. We view a lowering of control gains while maintaining pole locations as a desirable quality. Lower control gains will allow the system to operate in a linear region for larger error signals since actuator saturation will occur at larger error values. Additionally, they indicate that better performance, i.e., faster responses may be attainable at higher gains.

In making performance comparisons for a WIP, we are constrained by the dimensionality of the WIP control system. The Lagrangian equations and linearized system models with numerical values used in this paper are detailed in the Appendix for

reference. The linearized model for a WIP is a four state system (Eq. (A3) in the Appendix) which makes closed form analytical expressions exceedingly complex. Therefore, for analysis, we use numerical values given in the Appendix (Table 4). The procedure used to carry out our analysis is described below:

- (1) We form linearized state matrices by using the numerical values used in Table 4 (in the Appendix).
- (2) We then use the pole-placement technique to estimate feedback gains at fixed pole locations while varying parameters under study.

For consistency throughout this paper, we design all linearized controllers to have poles at locations given by Eq. (1). Note that any other pole location could be chosen for the same purpose and in our experience our numerical results remain valid as long as stable pole locations are chosen. Additionally, in analyzing various aspects of design discussed in this paper, we also present results from the simulation of an ideal WIP with no noise and actuator saturation. These theoretical simulations parallel our experimental observations and indicate that our results can be generalized to any WIP design:

$$\begin{aligned}
 p1 &= -7.0867 + 0.3005i \\
 p2 &= -7.0867 - 0.3005i \\
 p3 &= -1.2323 + 1.1338i \\
 p4 &= -1.2323 - 1.1338i
 \end{aligned} \tag{1}$$

To determine the relative performance of WIPs experimentally, we employ the phase diagram. Since the WIP has two degrees of freedom, pitch and wheel position, we analyze two separate phase portraits. These are pitch angle versus pitch rate and wheel position versus wheel velocity. Improved performance is indicated by smaller orbits, whereas larger orbits indicate large limit cycles in pitch and wheel position.

4 Effect of Tire Visco-Elasticity on Balancing Behavior

Visco-elasticity and other rolling phenomena in tires has been the subject of extensive research. An introductory survey of tire models is described by Fraggstedt [15]. Visco-elastic properties contribute to “damping” in rolling tires and are described by Stutts and Soedel [16]. Kim and Savkoor [17] examine three different damping models of tires. A document prepared by the NTSB [18] describes an increase in rolling resistance with speed and also describes the lowering of rolling resistance with temperature. It may be these two competing effects that reflect the common notion that rolling resistance is independent of speed [15]. Note that almost all studies on rolling tires were performed on vehicles designed to move faster than WIPs. To the best of our knowledge, the analysis presented by Thacker and Kauzlarich [19] for wheelchair tires is closest to what we desire for WIPs. The authors evaluate various models to estimate tire losses in wheelchairs coming to the conclusion that a combined hysteresis and visco-elastic loss model may be most appropriate. Based on this, for our analysis, we assume that tires exhibit an oppositional viscous torque to rolling motion at low velocities. To verify the accuracy of this assumption, we present experimental evidence subsequently.

We first describe analytically the basis for enhanced performance with soft tires. We then provide experimental evidence of viscous damping between soft tires and the ground while rolling and finally demonstrate reduced limit cycles when our experimental WIP, Charlie is balancing on soft tires. In addition to tire-ground damping, we also investigate drive train viscous friction in a similar manner and we will present both results in this section.

To model the effect of these damping terms, we derive the equations of motion with the following damping torques:

$$\tau_w = B_w \dot{\phi} \tag{2}$$

$$\tau_{wp} = B_{wp}(\dot{\phi} - \dot{\theta}) \quad (3)$$

where ϕ and θ are the angular positions of the wheel and the pendulum, respectively, as described in the Appendix. τ_w is the damping torque caused by the visco-elasticity of the tire and τ_{wp} is the torque due to the drive train. The equations of motion derived with these assumptions are given as follows:

$$\begin{aligned} -gLM_b \sin(\theta) + \ddot{\theta}(J_b + L^2M_b) + \dot{\theta}B_{wp} - \dot{\phi}B_{wp} + T &= 0 \quad (4) \\ (J_b + L^2M_b) \left(\ddot{\phi}(R^2(M_b + M_w) + J_w) + \dot{\phi}(B_w + B_{wp}) - \dot{\theta}B_{wp} - T \right) \\ - LRM_b \left(\dot{\theta}^2 \sin(\theta)(J_b + L^2M_b) + \cos(\theta)(\dot{\theta} - \dot{\phi}) + T \right) \\ + gL^2RM_b^2 \sin(\theta) \cos(\theta) &= 0 \quad (5) \end{aligned}$$

To analytically determine the effect of tire-ground and drive train damping, we vary B_w and B_{wp} in the range [0 1] while keeping the other zero and recomputing gains required to keep the poles in the locations p1, p2, p3, and p4 given by Eq. (1).

We see from Fig. 3 that tire-ground damping has a desirable effect. This is evident from the reduction in gains with increasing B_w and B_{wp} . Physically, we attribute this to the slower rate at which the WIP “falls” due to opposition to rolling in the tires. However, Fig. 3 does show a resonancelike peak but discounting this narrow spike in gain, which is a pole-zero elimination, increasing tire damping results in a general trend of reducing controller gains. Figures 3(e) and 3(f) also show the simulated output of the WIP to a disturbance. Note the reduction in the magnitude of the transient response when tire-ground damping is introduced.

4.1 Experimental Evidence of Tire Ground Damping. We have now described the analytical basis for increased performance

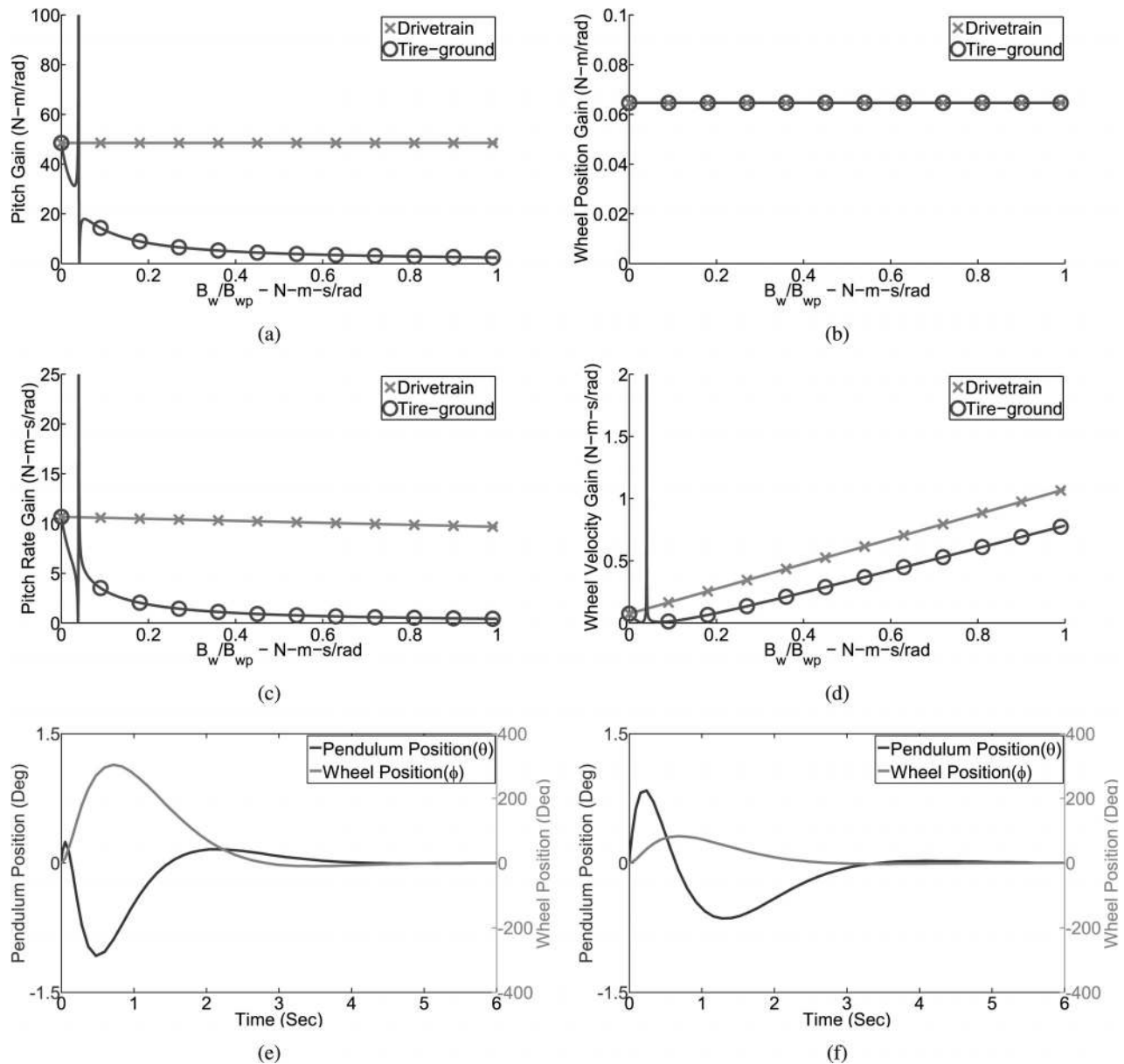


Fig. 3 The effect of tire damping (B_w) and drive train damping (B_{wp}) on pole-placement gains. Note that the X-axis represents the damping in both B_w and B_{wp} in all figures. (a) Comparison of pitch gains, (b) comparison of wheel position gains, (c) comparison of pitch rate gains, and (d) comparison of wheel velocity gains. The effect of tire-ground damping in simulation with an initial velocity of 0.1745 rad/s in pitch rate (e) $B_w = 0$ N m s/rad and (f) $B_w = 0.1$ N m s/rad.

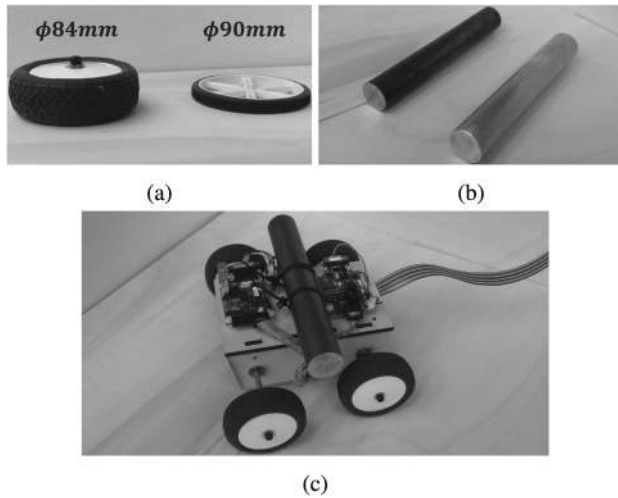


Fig. 4 Tire testing setup: (a) two tires were tested, 84 mm diameter on left and 90 mm diameter on right; (b) steel and aluminum rods of equal dimensions weighing 0.912 kg and 2.220 kg were loaded on the cart; and (c) cart instrumented with optical encoder to measure position and velocity

on account of tire–ground damping. In this section, we present experimental results that indicate the presence of viscous damping between tire and ground. To test tires for viscous damping, we use the experimental setup in Fig. 4. Figure 4(c) shows an instrumented cart with a steel bar as load. The cart is fitted with an optical encoder to capture position and velocity data.

We use this setup to test two types of tires, the tire on the left in Fig. 4(a) is a soft RC car tire with a foam insert, whereas the tire on the right is a stiff plastic wheel with a thin neoprene covering. To characterize the rolling behavior of either tire, we roll the cart down a 3 deg slope while recording position and velocity. The bearings supporting the axles in the cart have low viscous damping. To account for the possibility that the experiment may also capture effects of damping in bearings in addition to the tire–ground damping, we test the soft tires against the stiff plastic wheels. Hence, comparison between soft tires and hard wheels should yield contrasting results in spite of the damping at the bearings.

Our hypothesis is that if the soft tire exhibits viscous damping, then the velocity of the cart down the slope will be described by a two term exponential curve of the form given by Eq. (6). However, if there is very little tire–ground damping, the velocity versus time curve will be a straight line described by Eq. (7).

$$v = v_T(1 - e^{-Bt}) \quad (6)$$

$$v = g \sin(\theta) \times t \quad (7)$$

Figure 5 shows the results of our tests, each curve displayed is the average of three trials. In all cases, with no load, 0.912 kg, and 2.220 kg loads, the cart fitted with soft tires rolls slower. Additionally, the curves obtained using softer tires have an unmistakable exponential shape to them. A two term exponential also fits the data better than a straight line fit. This can be seen from Table 1 which shows the residual sum of squares (RSS) for both the exponential and linear fits. We see from the plots that the damping is also load dependent, with the cart rolling slower with increasing load.

4.2 Experimental Results—Performance of Soft Tires While Balancing. In Sec. 4.1, we established the viscous damping characteristics of tire–ground interactions. In this section, we present experimental evidence of enhanced performance of a WIP balancing on soft tires.

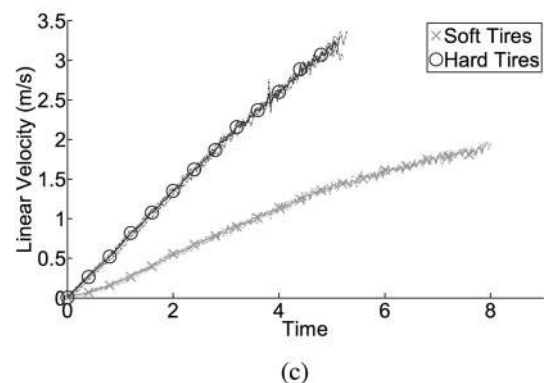
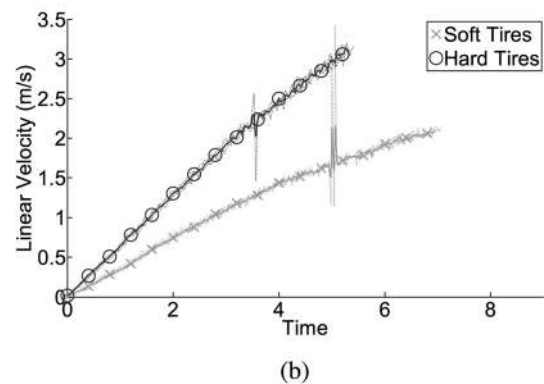
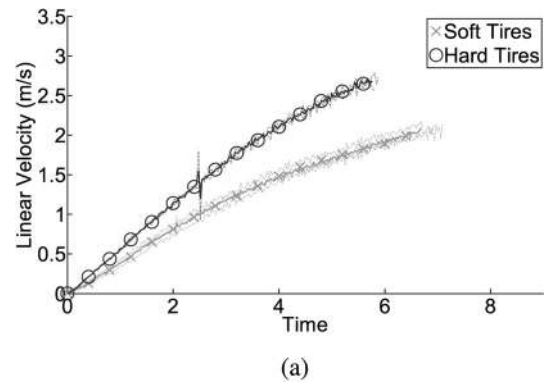


Fig. 5 Rolling resistance tests. (a) No load on cart, (b) cart loaded with 0.912 kg aluminum rod, and (c) cart loaded with 2.220 kg steel rod.

Table 1 RSS error for curves in Fig. 5

Curve	RSS—exponential fit	RSS—linear fit
No load soft tires	0.215712	4.886807
No load hard tires	0.449012	4.165307
0.912 kg soft tires	1.122077	4.189834
0.912 kg hard tires	0.277047	1.106508
2.220 kg soft tires	0.809054	3.584972
2.220 kg hard tires	0.169956	0.648381

To compare the performance of the WIP with soft tires and hard tires, we mount both tires on Charlie our experimental WIP and require the control loop to stabilize the pendulum at zero pitch angle and constant ground position. We then compare the phase portraits of both the wheel position and the pitch angle.

Figure 6 shows phase plots in pendulum and wheel positions for Charlie operated with both soft tires and hard plastic wheel. We see a substantial reduction in limit cycling behavior in

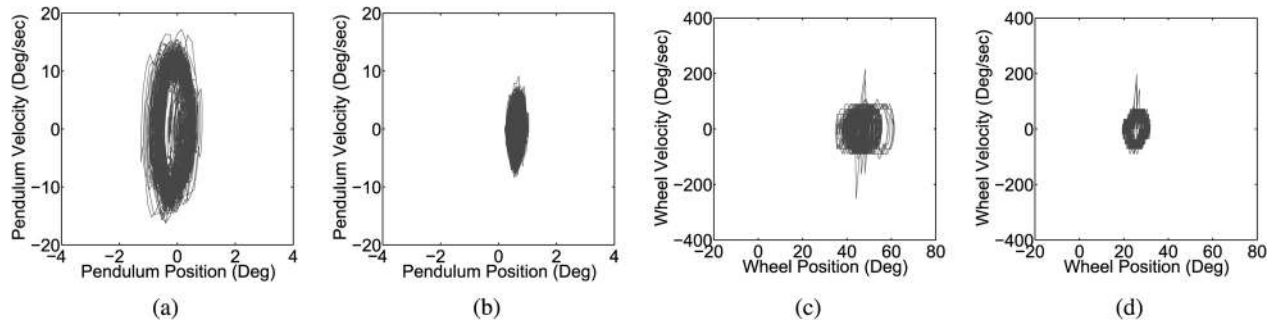
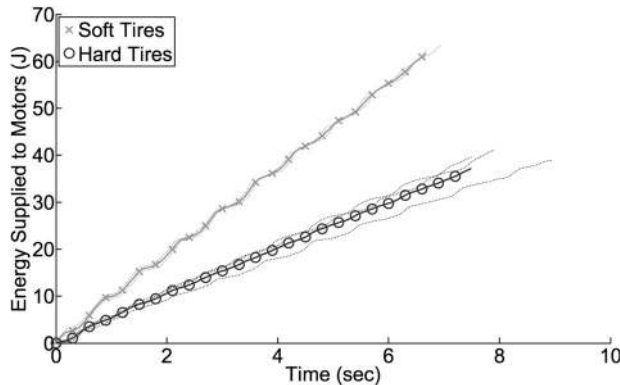
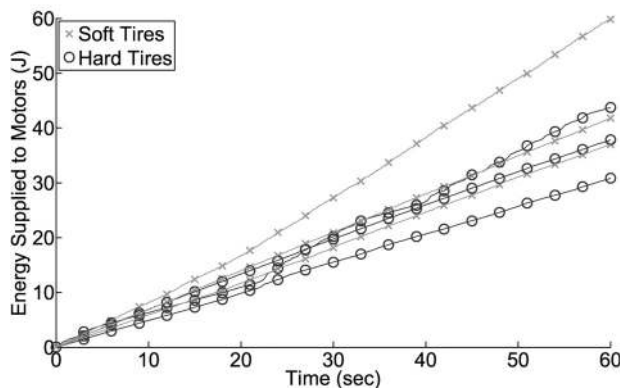


Fig. 6 Phase plots showing relative stability—(a) pendulum pitch versus pitch rate with hard tires, (b) pendulum pitch versus pitch rate with soft tires, (c) wheel position versus velocity with hard tires, and (d) wheel position versus velocity with soft tires



(a)



(b)

Fig. 7 Tire testing results. (a) Total energy supplied to motors for ground motion of 20π rad and (b) total energy supplied to motors to balance stationary for 30 s.

Figs. 6(b) and 6(d) compared to Figs. 6(a) and 6(c) which correspond to operation with soft tires and hard plastic wheels respectively.

4.3 Energetics of Soft Tires. In Sec. 4.2, we have shown that soft tires enhance the performance of a WIP, we now investigate the possible tradeoffs in using soft tires. We wish to investigate the energy cost of balancing on soft tires versus hard plastic wheels. To do this, we setup two experimental scenarios:

- (1) Charlie is commanded to move 10 wheel revolutions (20π rad) on horizontal ground. Figure 7(a) shows the energy consumed averaged over two trials, each using hard wheels and soft tires. The upper curve clearly shows that on soft tires, the robot consumes more energy.

- (2) Charlie balances in position for 60 s. Figure 7(b) shows the energy consumption for three trials each with soft tires and hard wheels. In this application, we see that the energy consumed by the robot does not differ noticeably on either set of tires.

Note that the energy supplied to the motors is computed as: $\sum_{n=0}^{60/T_s} V[n]I[n]T_s$, where T_s is the sampling time, V is the PWM voltage times the duty cycle, and I is the current. We see from the above experiments that the energy cost of using tires depends greatly on the intended application of the WIP.

In this section, we have seen that the visco-elastic nature of tires leads to a viscous damping torque between the tire and ground. Our analytical simulations as well as experiments point to an increase in performance with increasing tire-ground damping. We also see that there is a tradeoff between energy efficiency of the WIP and tire-ground damping; however, the extent of the tradeoff depends on the nature of the task executed by the WIP. For applications involving sustained motion, soft tires that exhibit tire-ground damping are less energy efficient than hard plastic tires. However, in applications that mostly involve holding position, there is no discernible difference in energy efficiency between soft tires and hard wheels. This is because the use of soft tires results in smaller wheel limit cycles resulting in reduced energy dissipation.

We believe that our results are extensible to pneumatic tires, which also exhibit visco-elastic deformations. In this case, however, tires inflated to a lower pressure would exhibit better performance and tires inflated to higher pressures would show more limit cycling. Our results also indicate that WIPs designed for continuous motion in open environments will have better energy efficiency with tires inflated to higher pressures; for stationary applications, the tires may be inflated to lower pressures for better limit cycle performance.

5 Effects of Velocity Filtering

In Sec. 4, we investigated the effect of tires on the stability of WIPs. In this section, we discuss velocity filtering. Wheel encoders are a common feature on WIPs and backward differences estimation is the preferred method of obtaining velocity values. However, this method of velocity estimation necessitates filtering to avoid noise. While one author avoids this problem by using analog quadrature encoders [7], this technique is not wide spread in its application. In this section, we demonstrate via simulation and experiments that it is not the filter cutoffs alone that matter. We show that a mismatch in filter cutoffs between the pitch rate and wheel velocity filters can introduce large limit cycles and instabilities in WIPs.

5.1 Simulation. To simulate the effect of low pass filtering of velocity in WIPs, we turn to the planar model described by Eqs. (A1) and (A2) (in the Appendix). Additionally, we introduce a

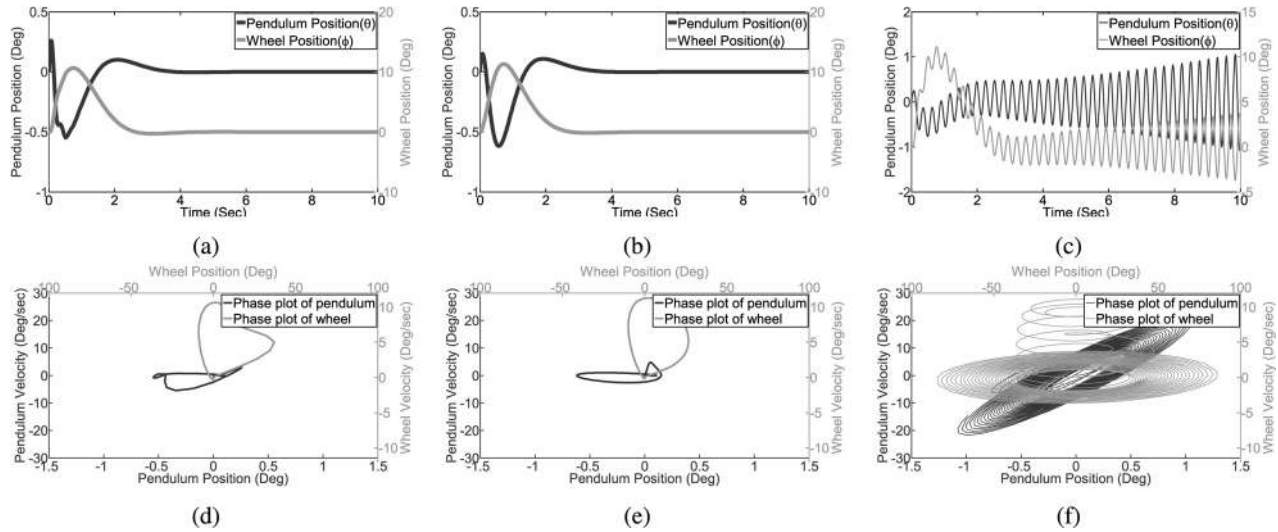


Fig. 8 Simulated output of WIP response to disturbance of 0.0873 rad/s in pitch rate under the following filter configurations. (a) and (d) Wheel velocity filter $f_c = 5.0$ Hz and pitch rate filter $f_c = 5.0$ Hz; (b) and (e) wheel velocity filter $f_c = 5.0$ Hz and pitch rate filter $f_c = 50.0$ Hz; (c) and (f) wheel velocity filter $f_c = 50.0$ Hz and pitch rate filter $f_c = 5.0$ Hz. Note the instability of the response in plots (c) and (f).

second order low pass butter filter for velocity signals $\dot{\theta}$ and $\dot{\phi}$. As we do with other simulations described in this paper, we design the linearized controller using pole placement techniques with poles at locations given by Eq. (1). Figure 8 shows the simulated response of the WIP to various filter cutoff frequencies. From the simulated results, it is interesting to note that matched filter cutoff frequencies for wheel velocity and pitch rate do not introduce instabilities in the balancing behavior. However, a mismatch between the pitch rate cutoff and the wheel velocity cutoff where the pitch rate cutoff is significantly lower than the pitch rate cutoff can introduce instabilities as well as limit cycles. To explore if this result will also extend to real WIPs, we setup appropriate filtering on our experimental WIP system. We describe the results in Sec. 5.2 below.

5.2 Experiments. To determine the effect of mismatch in filter frequency, we setup our experiment in the following manner. We implement two separate first order digital Butterworth filters for both the pitch rate and wheel velocity signals. While balancing at a fixed position, we measure both the pitch and pitch rate and the wheel position and wheel velocity for a 30 s period. We perform three trials each, with filter frequencies set at 9.69 Hz and 28.60 Hz, i.e., both filters at 9.69 Hz and then with filters at either 9.69 Hz or 28.60 Hz. The resulting phase plots are shown in Fig. 9. Note that while we simulated cutoff frequencies of 5 Hz and 50 Hz in Sec. 5.1, experimentally we start seeing limit cycles and instabilities as soon as we reduce the filter cutoffs to 9.69 Hz and 28.6 Hz. This difference is probably on account of parameter uncertainties and unmodeled nonlinearities.

We see that the experimental results in Fig. 9 are in broad agreement with the behavior predicted by simulations. We can see that the system is stable with both cutoff frequencies set to 9.69 Hz. However, Figs. 9(c) and 9(f) clearly show an unstable system when the cutoff of the wheel velocity filter cutoff is higher than the pitch rate filter cutoff.

Our analytical simulations indicate that the matching of pitch rate and velocity filters is essential to ensure good limit cycle performance. While setting a pitch rate filter cutoff lower than the wheel velocity cutoff can work under most conditions, there is a possibility of inducing limit cycles or instabilities. We believe that the important design implication from this section is that higher filter cutoffs do not necessarily contribute to stability

unless the frequency content in both the pitch and velocity rate signals is matched.

6 Limit Cycle Compensation for WIPs

In this section, we discuss another often encountered issue in WIPs, limit cycling. In practice, limit cycling is present in all WIPs; in this section, we focus on a strategy to minimize limit cycling behavior. A detailed look at the performance of the algorithm as well as the parameters affecting performance is given by Vasudevan et al. [20]. In this section, we explain the basic concepts of the algorithm and present experimental data, showing the reduction in limit cycling.

We note that in control systems designed for mechanical positioning, the most common source of limit cycles is friction. Olssen [21] describes the effect of friction in a classical inverted pendulum and cart setup. Campbell et al. [22] analyze limit cycles generated by the presence of stick-slip friction between the inverted pendulum cart and track and design a controller to stabilize the system. There is also research [23–26] that deals with methods to stabilize an inverted pendulum exhibiting frictional limit cycles. However, based on our observations, most friction compensation terms based on friction models in literature are complex and depend on numerical values of frictional parameters.

For WIPs, Akesson et al. [7] describe a method of compensation for coulomb friction. Our research focuses on automating the process of finding a compensation term (V_{fc}) added to the four state feedback equation (9) to minimize limit cycling. While Eq. (9) may look like friction compensation, the algorithm makes no attempt to model friction. Our method has been inspired by passivity-based approaches for haptic devices [27] and we borrow the idea of a “passivity” observer to measure the flow of power in and out of the system.

$$V_{uc} = K1(\theta - \theta_{des}) + K2(\phi - \phi_{des}) + K3\dot{\theta} + K4\dot{\phi} \quad (8)$$

$$V = V_{uc} + V_{fc}\text{sign}(V_{uc}) \quad (9)$$

To estimate the value of V_{fc} , we start by measuring the power supplied by the motors to the WIP. By observing the direction of power supplied to the two degrees of freedom of the system, we determine the type of limit cycle the WIP is executing. To do this, we evaluate two power products given as follows:

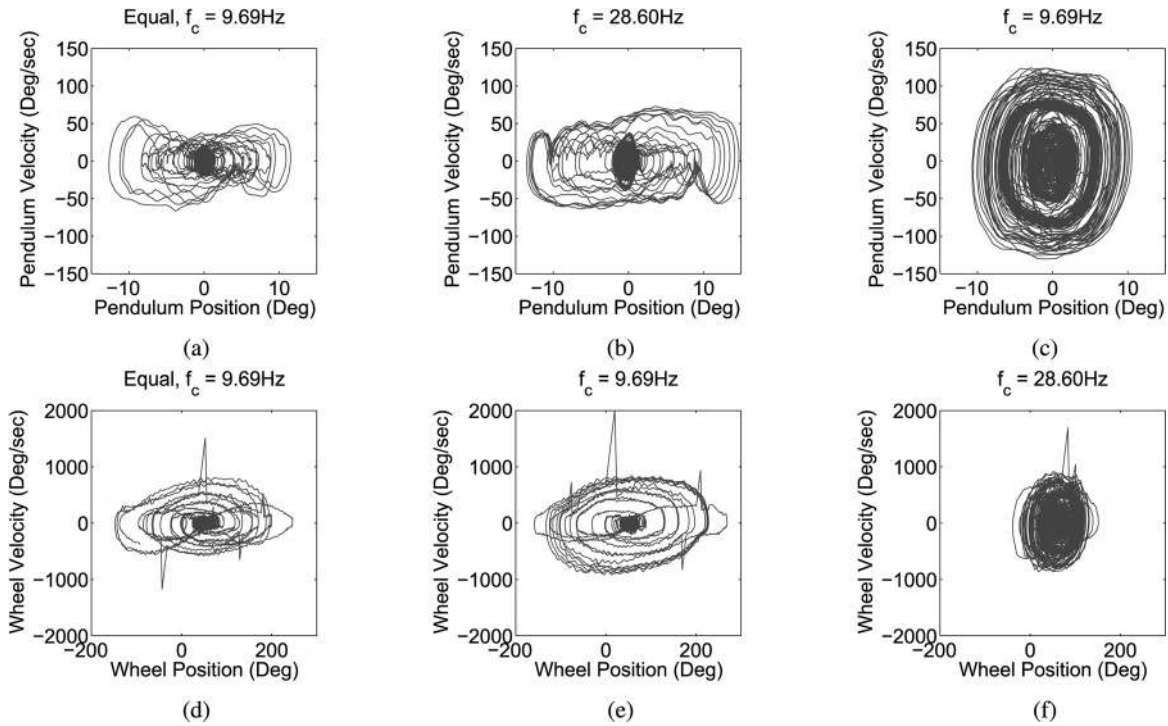


Fig. 9 (a)–(f) Phase plots with various filter configurations, filter cutoffs are indicated: (a) and (d) phase plots with equal cut off frequencies. (b), (e) and (c), (f) Phase plots with different cutoff frequencies.

$$P_p \propto \tau \dot{\theta} \propto V \dot{\theta} \quad (10)$$

$$P_w \propto \tau \dot{\phi} \propto V \dot{\phi} \quad (11)$$

Figure 10 shows the behavior of the WIP interpreted in terms of the sign of the power products, with the arrows showing the direction of motion of each degree of freedom. Figure 11 shows both the power products as well as the wheel and pendulum positions from experimental data. On the left side, we see limit cycles due to under-compensation. A close look at Fig. 11(a) shows that the pendulum mostly operates in quadrants III and IV. However, brief spikes of power into quadrants I and II result in limit cycles in pitch and wheel position. Our objective is to reduce limit cycling by minimizing operation in quadrants I and II.

Figure 11 also shows the effect of over-compensation on the right. An over-estimated V_{fc} term can also generate limit cycles, though of a different nature. The nature of power products during this type of limit cycle is markedly different and the power products exhibit an almost uniform distribution above and below zero. We use this difference in the nature of the power products between under-compensation and over-compensation to algorithmically tune the compensation term to minimize limit cycles. The algorithm is described in Fig. 12(a) and Table 2 explains the parameters in the algorithm. The algorithm works by increasing the compensation term (V_{fc}) if the WIP operates in quadrants I and II and by decreasing the compensation term if the power products exhibit symmetry about the zero line and exceed a threshold power ($P_{Th\delta}$). A phase plot showing the reduction in limit cycling during the runtime of the algorithm is given in Fig. 12(b)

The main advantage of the algorithm presented in this section is its robustness to parameter variations in WIPs such as tensioner variability, battery voltage, etc. Its implementation is simple and can be an easy addition to common full state feedback controllers employed in WIPs.

7 Effect of Voltage Versus Current Control

In design of control systems for WIPs, DC electric motors are usually the primary actuators. Two control techniques for DC motors are current (or torque) control and voltage (or velocity) control. A WIP design must implement either of these control paradigms and in this section we present results that indicate that the voltage controlled motors may offer a simpler alternative while maintaining the same performance as current controlled motors.

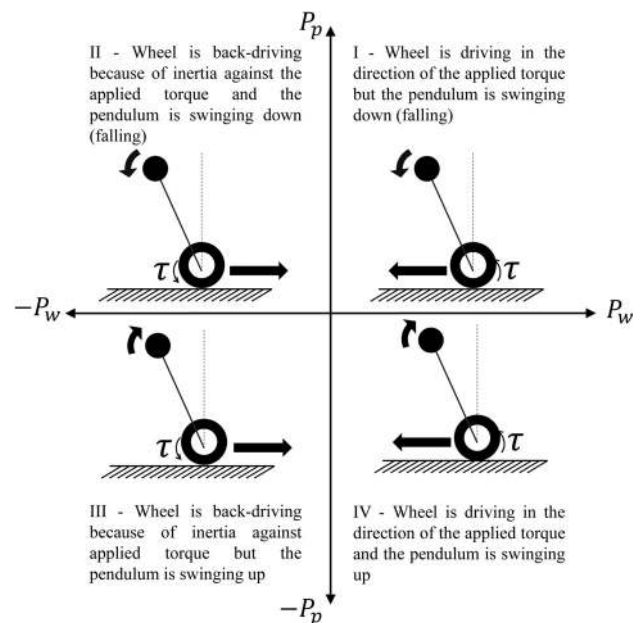


Fig. 10 Interpretation of the behavior of the balancing machine based on the sign of mechanical power terms, quadrants III and IV represent stabilizing conditions

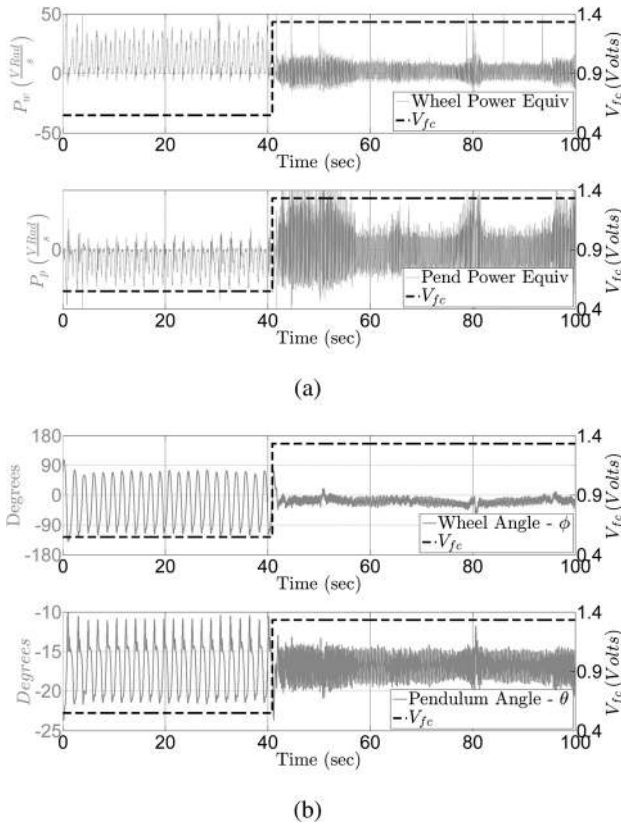


Fig. 11 Two types of limit cycle behavior depending on the magnitude of the compensation term, V_{fc} . From 0 to 40 s, the plots display limit cycles generated due to an underestimation of V_{fc} while from 40 to 100 s limit cycles due to an overestimation of V_{fc} are displayed. (a) Wheel and pendulum power products. The negative spikes in P_w and positive spikes of P_p between 0 and 40 s indicate deviation quadrants IV and III, and (b) pitch and wheel positions.

A majority of WIP platforms in research have implemented current controllers [3,5,9] while voltage controlled platforms [7] are fewer. Equation (13) along with Table 3 shows a simple model that ignores motor inductance. We also note that numerically $k_e = k_t$, as we shall use this in our simulations later in this section.

Table 2 Parameters in limit cycle compensation algorithm

Parameter	Description
P_{Thp}	Noise threshold in pendulum power-equivalent product
$V_{fc}(t)$	Friction compensation term to be estimated
Δ	Amount to increment or decrement from the friction compensation term
δ	Time window to perform averaging of samples, i.e., number of samples to keep in memory
$P_{Th\delta}$	Threshold for average energy output from the system over the last δ samples

Table 3 Parameters in DC motor in Eq. (13)

Parameter	Description
i	Current through armature (A)
R_a	Resistance of armature (5.0 Ω)
k_e	Voltage constant of motor (V s/rad)
k_t	Torque constant of motor (A s/rad)
ω	Angular velocity of motor (rad/s)

Equations (12) and (13) are the basis for the control of DC motors. Equation (13) represents the voltage control of DC motors. In this case, the torque output is influenced by the back-emf due to rotor motion. Torque control for DC motors requires a current feedback control system to maintain a constant armature current which can be implemented with either an analog or digital control loop. In practice, at large angular velocities, this control loop can saturate and back emf effects can still appear. However, in our analysis, we will assume a perfect torque control system. Equation (12) therefore describes the ideal current controller.

$$T = k_t i \quad (12)$$

$$T = \frac{k_t}{R_a} (V - k_e \omega) \quad (13)$$

To study the effect of the two motor control techniques on WIP performance, we set up the following analytical simulation. The dynamic equation of WIP control under torque or voltage control paradigm is formed by Eqs. (12) and (13) substituted into the dynamic equations of the WIP defined by Eq. (A2) and

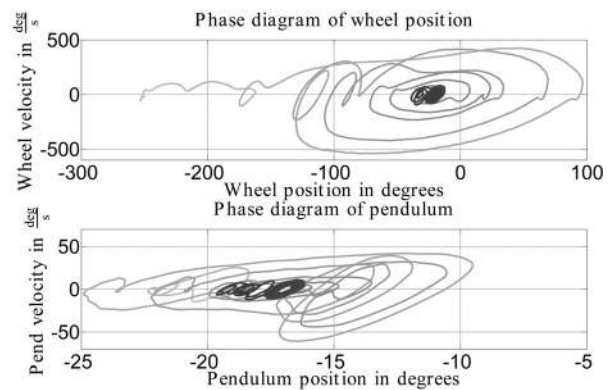
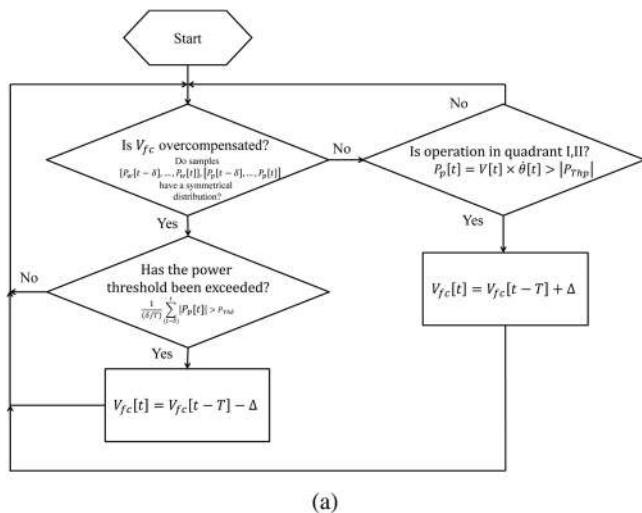


Fig. 12 (a) Friction compensation algorithm and (b) phase plot of operation of compensation algorithm. Time is encoded in color with red representing $t = 0$ s and blending into dark gray at $t = 35$ s. Note the reduction in limit cycles indicated by small central dark gray orbit.

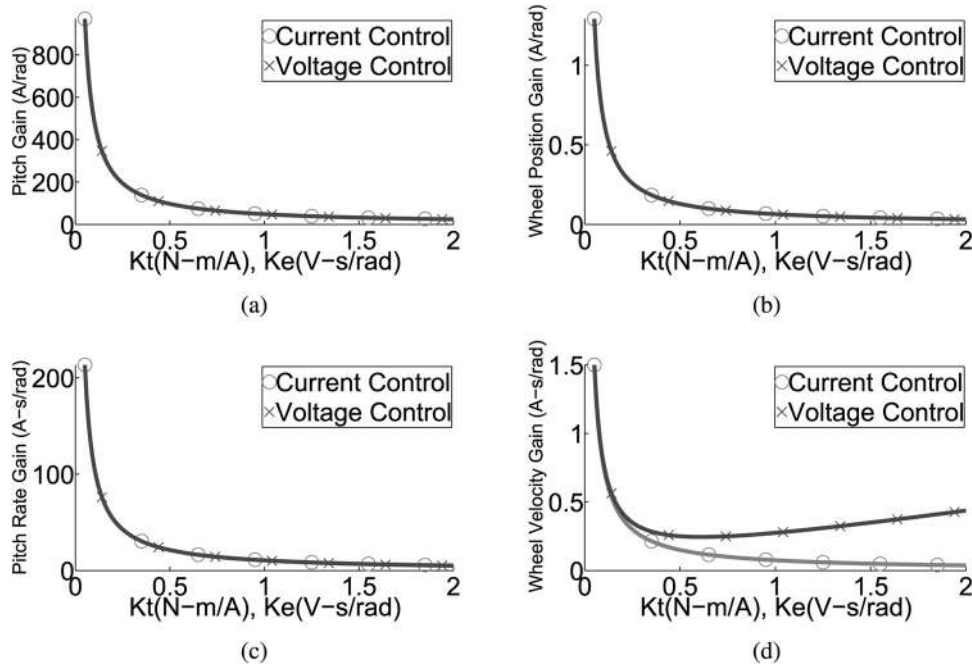


Fig. 13 (a) Variation of pitch gain with motor constants, (b) variation of wheel position gain with motor constants, (c) variation of pitch rate gain with motor constants, and (d) variation of wheel velocity gain with motor constants. Note: the wheel velocity gain is the only gain that reduces the stability margin of the voltage controlled WIP.

subsequently linearized into Eqs. (A4) and (A5) (in the Appendix). Now we compare change in feedback gains for motors of various torque and back-emf capabilities by varying motor constants $k_e = k_t$ while fixing closed loop pole positions (Eq. (1)). The feedback gains for torque control have the dimensions (A/rad, A s/rad) and feedback gains for current control have dimensions (V/rad, V s/rad), making a direct comparison difficult. To work around this problem, we modify the voltage control feedback gains ($K_{v1}, K_{v2}, K_{v3}, K_{v4}$) to ($K_{v1}/R_a, K_{v2}/R_a, K_{v3}/R_a, K_{v4}/R_a$). This ensures that we are making a correct dimensional comparison, while numerically corresponding to the “stall” current of a DC motor:

$$\begin{aligned}
 p1 &= -7.0867 + 0.3005i \\
 p2 &= -7.0867 - 0.3005i \\
 p3 &= -1.2323 + 1.1338i \\
 p4 &= -1.2323 - 1.1338i
 \end{aligned}
 \tag{14}$$

We see from Fig. 13 that three of the four gains required are identical between torque and velocity control schemes. The wheel velocity gain is the only gain that shows variation between the two control schemes. Given the similarity in performance, we argue that velocity control is preferable for simplicity in implementation. We can infer from the lower values for wheel velocity gains that current control may present an alternative for WIPs designed for high speed where back-emf effects are significant. In other cases, the complexity of implementing either additional analog circuitry or a high speed digital control loop makes the simpler velocity control a more attractive alternative.

8 Effect of Motor Gearing

As the results from our study of voltage and current control indicate, a sufficient actuator torque is required to maintain adequate balancing performance. However, there are two methods of achieving high actuator torque—by employing larger and more

expensive motors or by using an appropriately sized gearhead. In this section, we investigate the effect of employing gearing to achieve appropriate actuator torque.

The numerical values of parameters used in this analytical simulation are described in Table 4. To analyze the effect of gearing, we include amplification of rotor inertia, torque, and back-emf effects. This is given by Eqs. (15)–(17). Additionally, we fix the closed loop poles at locations given by Eq. (14) and simulate a voltage controlled motor (Eq. (A4), in the Appendix). The results of the simulation are shown in Fig. 14.

$$J_{wEff} = J_w + J_m N^2 \tag{15}$$

$$k_e = k_e N \tag{16}$$

$$k_t = k_t N \tag{17}$$

We see that at low gearing ratios, very large gains are required to stabilize the WIP, this can be attributed to the insufficiency of actuator torque. However, the curves even out very soon and the wheel and wheel velocity gains show a steady increase with increasing gearing ratios on the right side of the graph. To demonstrate the advantages of higher gearing, Figs. 14(e) and 14(f) shows the simulated response of a WIP to a disturbance of 0.1745 rad/s in pitch rate. Note the magnitude of overshoot of the WIP with a gearing of 200:1 as compared to the WIP with 50:1 gearing.

The analysis presented in this section indicates that if only balancing in position is to be achieved then gearing a low torque motor is an acceptable solution. While the simulation shows that an increase in gearing ratio is a good solution for WIPs, in practice increasing the gearing ratio comes with some associated problems. Primarily, the performance of the balancing system will not be robust as large ratio gear boxes offer significant friction and backlash resulting in limit cycling and backlash chattering. Additionally, if the WIP is designed for applications that require motion, then back-emf and reflected inertia effects will reduce the balancing performance of the WIP. Another result apparent from

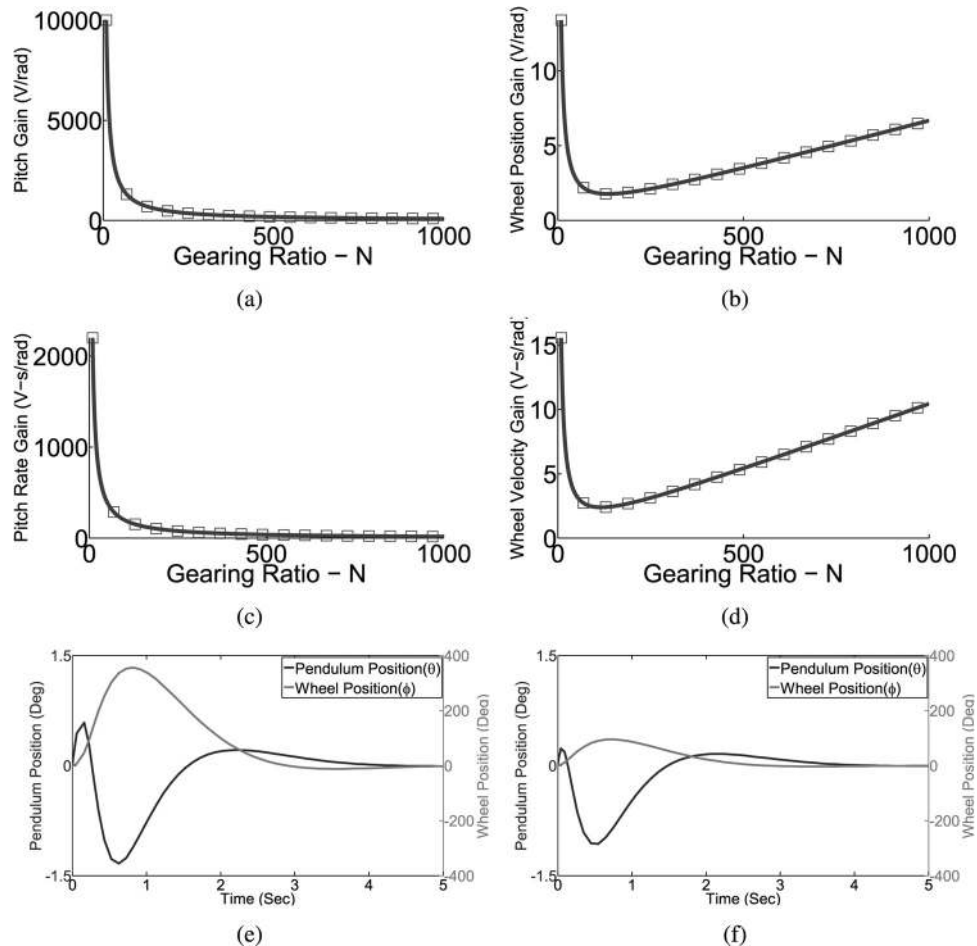


Fig. 14 (a) Pitch gain variation with gearing ratio, (b) wheel position gain with gearing ratio, (c) pitch rate gain with gearing ratio, (d) wheel velocity gain with gearing ratio, and (e) and (f) simulation of WIP response to a disturbance of 0.1745 rad/s in pitch rate with gearing ratios $N=50$ and $N=200$

the simulation is that once the required torque to balance a WIP is achieved, further increase in actuator torque does not enhance performance. This is inferred from the asymptotic nature of the curves in Fig. 14.

9 Conclusions and Future Work

We have described a number of experiments, analytical simulations, and results in this paper. In this section, we distill our results into design recommendations for WIP design:

- (1) From our investigations, we conclude that the selection of tires greatly affects WIP performance. If the WIP is designed to hold position, then soft tires or pneumatic tires inflated to a low pressure are recommended as this contributes greatly to balancing performance. If on the other hand, the WIP is designed for constant motion, then hard tires or pneumatic tires at high pressure are desirable as they offer greater energy efficiency.
- (2) The performance of the WIP is affected by the frequency content in the pitch rate and wheel velocity signals. We recommend equal filter cutoffs for both these signals as this will result in superior balancing performance. Specifically, we have seen that a low cutoff frequency for the pitch rate and high cutoff frequency for the wheel velocity results in an unstable or limit cycling WIP.
- (3) We introduce a limit cycle compensation algorithm for WIPs that is simple in structure and easy to implement. The

algorithm is robust to parameter variations and automatically minimizes limit cycle behavior.

- (4) We have presented results indicating that voltage control of DC motors in WIPs offers the same balancing performance as current control for a lower design complexity/cost. We also describe the case of WIPs designed for high speeds where back-emf effects may make current control preferable.
- (5) We have shown that increasing the motor gearing ratio as a method for achieving balancing torque is a feasible solution. However, we also note that it is a less robust solution as it is prone to backlash chattering and limit cycling.

While our results do not constitute rigorous mathematical proofs, we hope that through our simulations and experiments we can offer some insight into important aspects of WIP design. Our final aim to assist the designer of a new WIP system faced with numerous design decisions in making choices about various sub-components faster and with adequate knowledge of tradeoffs inherent in any engineering design.

In the future, we wish to explore other aspects of WIP design. For example, backlash chattering in WIP gearboxes is a phenomenon that limits the maximum achievable stable gain. Additionally, we believe that the structural bandwidth of the WIPs plays a role in determining balancing behavior. Knowledge of structural bandwidth can determine the optimal placement of the accelerometer and rate-gyro sensor. We hope to address these research questions in the future.

Appendix: WIP Mode and Linearized State Equations

The dynamics for the WIP have been covered in a number of papers [5,28,29] and hence we do not present the full derivation. Equations (A1) and (A2) are derived from the Lagrangian equations of the system illustrated in Fig. 15. The definitions of various parameters in Fig. 15 are described in Table 4. The table also contains values of other numerical parameters used in analytical simulations.

Linearized state matrices used in Sec. 4 are given by Eq. (A3). These equations are used to determine effect of soft tires on stability. Linearized state matrices used in Sec. 7 are given by Eq. (A5) for current control and Eq. (A4) for voltage control.

$$-gL M_b \sin(\theta) + \ddot{\theta}(J_b + L^2 M_b) + T = 0 \quad (\text{A1})$$

$$g L^2 R M_b^2 \sin(\theta) \cos(\theta) + (J_b + L^2 M_b) \left(\ddot{\phi} (R^2 (M_b + M_w) + J_w) - T \right) \times -LR M_b \left(\dot{\theta}^2 \sin(\theta) (J_b + L^2 M_b) + T \cos(\theta) \right) = 0 \quad (\text{A2})$$

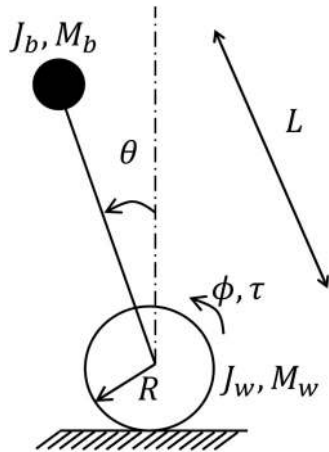


Fig. 15 WIP model

Table 4 Simulation parameters

Parameter	Definition	Value
M_b	Mass of body	4.5 kg
M_w	Mass of wheel	50×10^{-3} kg
L	Distance from center of mass of wheel to center of mass of body	19.2×10^{-2} m
R	Radius of wheel	45×10^{-3} m
J_b	Inertia of body: $M_b \times (L + R)^2$	25.28×10^{-2} kg m ²
J_w	Inertia of wheel: $M_w \times R^2/2$	5.0625×10^{-5} kg m ²
J_m	Inertia of rotor	5.0625×10^{-07} kg m ²
$K_t = K_e$	Torque and voltage constants for motor	$2.694 \times 10^{-3} \frac{\text{As}}{\text{rad rad}}$
T_s	Sampling time	0.01 s
Θ	Angle between the WIP and vertical or pitch	
ϕ	Angle between wheel and vertical	
$\dot{\theta}$	Rate of change of θ or pitch rate	
$\dot{\phi}$	Wheel velocity	
T	Torque exerted between the body and the wheel	

$$a_{21} = \frac{gL M_b}{J_b + L^2 M_b}$$

$$a_{22M1} = -\frac{B_{wp}}{J_b + L^2 M_b}$$

$$a_{22M2} = -\frac{K_e K_t}{R_a (J_b + L^2 M_b)}$$

$$a_{24M1} = \frac{B_{wp}}{J_b + L^2 M_b}$$

$$a_{24M2} = \frac{K_e K_t}{R_a (J_b + L^2 M_b)}$$

$$a_{41} = -\frac{gL^2 R M_b^2}{(J_b + L^2 M_b)(R^2 (M_b + M_w) + J_w)}$$

$$a_{42M1} = \frac{B_{wp} (J_b + L M_b (L + R))}{(J_b + L^2 M_b)(R^2 (M_b + M_w) + J_w)}$$

$$a_{42M2} = \frac{K_e K_t (J_b + L M_b (L + R))}{R_a (J_b + L^2 M_b)(R^2 (M_b + M_w) + J_m + J_w)}$$

$$a_{44M1} = -\frac{J_b (B_w + B_{wp}) + L M_b (B_{wp} (L + R) + L B_w)}{(J_b + L^2 M_b)(R^2 (M_b + M_w) + J_w)}$$

$$a_{44M2} = -\frac{K_e K_t (J_b + L M_b (L + R))}{R_a (J_b + L^2 M_b)(R^2 (M_b + M_w) + J_m + J_w)}$$

$$b_{21} = -\frac{1}{J_b + L^2 M_b}$$

$$b_{41} = \frac{J_b + L M_b (L + R)}{(J_b + L^2 M_b)(R^2 (M_b + M_w) + J_w)}$$

$$\begin{pmatrix} A & B \\ C & D \end{pmatrix} = \begin{pmatrix} 0 & 0 & 1 & 0 & 0 \\ a_{21} & a_{22M1} & 0 & a_{24M1} & b_{21} \\ 0 & 0 & 0 & 1 & 0 \\ a_{41} & a_{42M1} & 0 & a_{44M1} & b_{41} \\ 1 & 0 & 0 & 0 & 0 \\ 0 & 1 & 0 & 0 & 0 \\ 0 & 0 & 1 & 0 & 0 \\ 0 & 0 & 0 & 1 & 0 \end{pmatrix} \quad (\text{A3})$$

$$\begin{pmatrix} A & B \\ C & D \end{pmatrix} = \begin{pmatrix} 0 & 0 & 1 & 0 & 0 \\ a_{21} & a_{22M2} & 0 & a_{24M2} & \frac{K_t}{R_a} b_{21} \\ 0 & 0 & 0 & 1 & 0 \\ a_{41} & a_{42M2} & 0 & a_{44M2} & \frac{K_t}{R_a} b_{41} \\ 1 & 0 & 0 & 0 & 0 \\ 0 & 1 & 0 & 0 & 0 \\ 0 & 0 & 1 & 0 & 0 \\ 0 & 0 & 0 & 1 & 0 \end{pmatrix} \quad (\text{A4})$$

$$\begin{pmatrix} A & B \\ C & D \end{pmatrix} = \begin{pmatrix} 0 & 0 & 1 & 0 & 0 \\ a_{21} & 0 & 0 & 0 & k_t b_{21} \\ 0 & 0 & 0 & 1 & 0 \\ a_{41} & 0 & 0 & 0 & k_t b_{41} \\ 1 & 0 & 0 & 0 & 0 \\ 0 & 1 & 0 & 0 & 0 \\ 0 & 0 & 1 & 0 & 0 \\ 0 & 0 & 0 & 1 & 0 \end{pmatrix} \quad (\text{A5})$$

References

- [1] Segway, Inc., Bedford, NH, <http://www.segway.com/>
- [2] Nguyen, H. G., Morrell, A. J., Mullens, B. K., Burmeister, A. A., Miles, S., Farrington, C. N., Thomas, A. K., and Gage, D. W., 2004, "Segway Robotic Mobility Platform," SPIE Mobile Robots XVII, Philadelphia, PA, October 27–28.
- [3] Nakajima, R., Tsubouchi, T., Yuta, S., and Koyanagi, E., 1997, "A Development of a New Mechanism of an Autonomous Unicycle," IEEE/RSJ International Conference on Intelligent Robots and Systems (IROS'97), Grenoble, France, Sept. 7–11, pp. 906–912.
- [4] Ha, Y., and Yuta, S., 1994, "Trajectory Tracking Control for Navigation of Self-Contained Mobile Inverse Pendulum," IEEE/RSJ/GI International Conference on Intelligent Robots and Systems (IROS'94), "Advanced Robotic Systems and the Real World," Munich, Germany, Sept. 12–16, pp. 1875–1882.
- [5] Grasser, F., D'Arrigo, A., Colombi, S., and Rufer, A., 2002, "Joe: A Mobile, Inverted Pendulum," IEEE Trans Ind. Electron., 49(1), pp. 107–114.
- [6] Baloh, M., and Parent, M., 2003, "Modeling and Model Verification of an Intelligent Self-Balancing Two-Wheeled Vehicle for an Autonomous Urban Transportation System," International Conference on Computational Intelligence, Robotics, and Autonomous Systems. (CIRAS2003), Singapore, Taiwan, Dec. 15–18.
- [7] Akesson, J., Blomdell, A., and Braun, R., 2005, "Design and Control of YAIP—An Inverted Pendulum on Two Wheels Robot," Computer Aided Control System Design, IEEE International Conference on Control Applications and IEEE International Symposium on Intelligent Control (CADSD-CCA-ISIC), Munich, Germany, Oct. 4–6, pp. 2178–2183.
- [8] Lauwers, T., Kantor, G., and Hollis, R., 2005, "One is Enough," 12th International Symposium of Robotics Research, San Francisco, Oct. 12–15, pp. 12–15.
- [9] Lauwers, T. B., Kantor, G. A., and Hollis, R. L., 2006, "A Dynamically Stable Single-Wheeled Mobile Robot With Inverse Mouse-Ball Drive," IEEE International Conference on Robotics and Automation, (ICRA 2006), Orlando, FL, May 15–19, pp. 2884–2889.
- [10] Nagarajan, U., Kantor, G., and Hollis, R. L., 2009, "Human–Robot Physical Interaction With Dynamically Stable Mobile Robots," 4th ACM/IEEE International Conference on Human Robot Interaction (HRI 2009), La Jolla, CA, Mar. 11–13, pp. 281–282.
- [11] Yang, C., Li, Z., and Li, J., 2013, "Trajectory Planning and Optimized Adaptive Control for a Class of Wheeled Inverted Pendulum Vehicle Models," IEEE Trans. Cybern., 43(1), pp. 24–36.
- [12] Li, Z., and Yang, C., 2012, "Neural-Adaptive Output Feedback Control of a Class of Transportation Vehicles Based on Wheeled Inverted Pendulum Models," IEEE Trans. Control Systems Technology, 20(6), pp. 1583–1591.
- [13] Li, Z., and Zhang, Y., 2010, "Robust Adaptive Motion/Force Control for Wheeled Inverted Pendulums," Automatica, 46(8), pp. 1346–1353.
- [14] Li, Z., Zhang, Y., and Yang, Y., 2010, "Support Vector Machine Optimal Control for Mobile Wheeled Inverted Pendulums With Unmodelled Dynamics," Neurocomputing, 73(13–15), pp. 2773–2782.
- [15] Fraggstedt, M., 2008, "Vibrations, Damping and Power Dissipation in Car Tyres," Ph.D. thesis, Marcus Wallenberg Laboratory, Royal Institute of Technology, Stockholm, Sweden.
- [16] Stutts, D. S., and Soedel, W., 1992, "A Simplified Dynamic Model of the Effect of Internal Damping on the Rolling Resistance in Pneumatic Tires," J. Sound Vib., 155(1), pp. 153–164.
- [17] Kim, S.-J., and Savkoor, A. R., 1997, "The Contact Problem of In-Plane Rolling of Tires on a Flat Road," Veh. Syst. Dyn., 27(Suppl. 001), pp. 189–206.
- [18] Clark, S. K., and U.S. National Highway Traffic Safety Administration, 1981, "Mechanics of Pneumatic Tires," U.S. Department of Transportation, National Highway Traffic Safety Administration, Washington, DC, DOT HS 805 952, pp. 592–594.
- [19] Kauzlarich, J. J., and Thacker, J. G., 1985, "Wheelchair Tire Rolling Resistance and Fatigue," J. Rehabil. Res. Dev., 22(3), pp. 25–41.
- [20] Vasudevan, H., Dollar, A. M., and Morrell, J. B., 2013, "Energy-Based Limit Cycle Compensation for Dynamically Balancing Wheeled Inverted Pendulum Machines," ASME Paper No. DSCC2013-3843.
- [21] Olsson, H., 1996, "Control Systems With Friction," Institutionen för reglerteknik, Lunds tekniska högskola. Department of Automatic Control, Lund Institute of Technology, Lund, Sweden.
- [22] Campbell, S. A., Crawford, S., and Morris, K., 2008, "Friction and the Inverted Pendulum Stabilization Problem," ASME J. Dyn. Syst., Meas., Control, 130(5), p. 054502.
- [23] Aimar, R., Indri, M., Stomboli, T., and Bona, B., 1995, "Experiments on Robust Friction Compensation: The Inverted Pendulum Case," American Control Conference, Seattle, WA, June 21–23, pp. 3303–3305.
- [24] Chang, L.-H., and Lee, A.-C., 2007, "Design of Nonlinear Controller for Bi-Axial Inverted Pendulum System," IET Control Theory Appl., 1(4), pp. 979–986.
- [25] Ostertag, E., and Carvalho-Ostertag, M. J., 1993, "Fuzzy Control of an Inverted Pendulum With Fuzzy Compensation of Friction Forces," Int. J. Syst. Sci., 24(10), pp. 1915–1921.
- [26] Medrano-Cersa, G., 1999, "Robust Computer Control of an Inverted Pendulum," IEEE Control Syst., 19(3), pp. 58–67.
- [27] Hannaford, B., and Ryu, J.-H., 2002, "Time-Domain Passivity Control of Haptic Interfaces," IEEE Trans. Rob. Autom., 18(1), pp. 1–10.
- [28] Pathak, K., Franch, J., and Agrawal, S., 2005, "Velocity and Position Control of a Wheeled Inverted Pendulum by Partial Feedback Linearization," IEEE Trans. Rob., 21(3), pp. 505–513.
- [29] Li, Z., Yang, C., and Fan, L., 2013, Advanced Control of Wheeled Inverted Pendulum Systems, Springer-Verlag, London.